Sodium guidestar signal levels measured at AMOS and comparison to theory

D. Senft[1], B. Hunt[1], T. Swindle[1], N. Morris[1], R. Holmes[2], E. Walker[2], J. Lucas[2], J. Toth[2], M. Abercrombie[2], J. Mooney[2], T. Georges[2]

1 Air Force Research Laboratory, 550 Lipoa Avenue, Kihei, HI 96753

2 Boeing Laser Technical Services, , Kihei, HI 96753

ABSTRACT

On-sky testing of the continuous-wave (CW) sodium guidestar at the AMOS (Advanced Maui Optical and Supercomputer Site) site located atop Mount Haleakala, HI involved collections from March 2018 to March 2019 and have been compared with theoretical expectations. Sodium-beacon photon returns were measured with wavefront sensors on the 3.6m AEOS telescope. In addition, launch telescope and main telescope transmission was estimated from earlier collections from stars. Detailed comparisons of sodium return signals to theory properly account for atmospheric and optical transmission, sodium and laser linewidths, laser tuning to sodium line, laser polarization, population saturation, superflourescence, and geomagnetic field effects. Adaptive optics performance implications are discussed.

1. INTRODUCTION

The sodium laser guidestar (LGS) approach has been known for many years and is implemented or planned for implementation on most modern large astronomical telescopes [1-11]. The use of the sodium layer is especially beneficial, since its longer range and relatively high signal levels can provide superior correction of the atmosphere with adaptive optics. However, the sodium layer requires that the laser spectral line shape be well-matched to the sodium layer line, which is inhomogeneously broadened due to thermal motion of the sodium atoms. The nominal Doppler-broadened linewidth is 1.2 GHz, full-width at half max (FWHM) [1-3]. The natural linewidth of the sodium D_2 line is much narrower, about 62 MHz (FWHM) corresponding to a lifetime of about 16.3 nanoseconds [1-3, 13] Because the laser linewidth is much less than the natural linewidth, only those atoms that are within ± 62/2 MHz of the center of the laser line will be excited. In such cases, the concentration of laser energy can potentially saturate that narrow population of sodium atoms. Analyses of these effects follow. There are also polarization, optical pumping, and geomagnetic field effects [1-3, 14]. These will also be considered herein.

Fig. 1 shows the observation of Rayleigh and sodium backscatter on the Large Area Acquisition Telescope (LAAT) at the edge of the Advanced Electro-Optical System (AEOS) telescope. It is seen that the cone of Rayleigh backscatter dominates the scene, and that there is a limited angular region between that cone and the sodium layer spot.

Fig. 2 shows the observation of the sodium fluorescence backscatter on the Long-Range Imaging Lidar (LRIL) Atmospheric Wavefront Sensor (AWFS) during early observations in November 2017, and also 14 months later. The LGS initially had significant aberrations, primarily focus and astigmatism, which is evidenced in the left figure by large and irregular spots. After correction of these launch-telescope aberrations in January 2018, the spots were observed to look more like those on the right. After a few months of poor weather, testing began in March 2018, and results are shown for 13 months of results, from March 2018 to March 2019.

This paper is organized as follows. Section 2, Analysis, estimates the expected spot size and signal levels on the wavefront sensor. This section also characterizes the expected signal in photons/sec/cm2/W at the telescope pupil, which is a property of the sodium layer and the site. Section 3 summarizes signal levels by month starting in March 2018 through March 2019. Section 4 discusses the results and identifies potential means for further signal improvements. Section 5 summarizes the paper and includes recommendations.

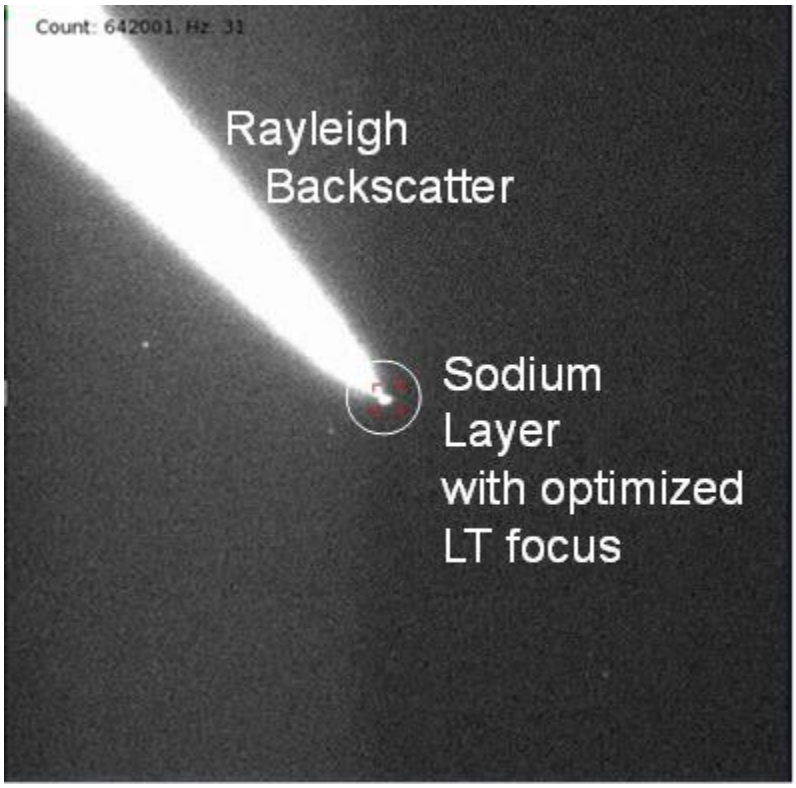

Fig. 1. Rayleigh and Sodium backscatter as observed on the LAAT.

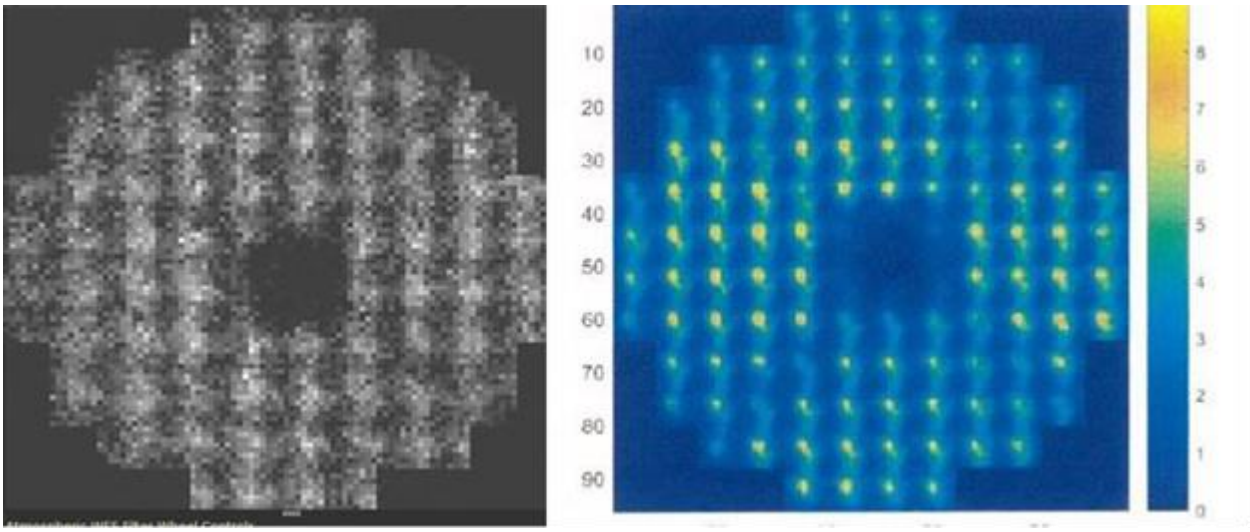

Fig. 2. Sodium fluorescence backscatter on the LRIL Atmospheric Wavefront Sensor, Left: Nov. 2017. Right: Jan 2019.

2. ANALYSES

The average column density for the sodium layer at Haleakala is estimated to be $4.3\pm1.1\text{x}10^9$ sodium atoms/cm^2 [17]. In the simplest analysis, the mean number of photoelectrons resulting from the resonant sodium backscatter into a subaperture per integration time, S_{Na0}, is [1-2]:

$$S_{Na0} = C_{Na}\, N_c\, T_A^2\, T_u\, T_d\, QE\, P_L\, D_{subap}^2\, \tau_{int}, \quad (1)$$

where

S_{Na0} = expected number of photoelectrons resulting from the resonant sodium backscatter into a subaperture per integration time, neglecting all degrading effects except atmospheric transmission at zenith

C_{Na} = leading factor from Eq. (27) of [2] (3×10^{-8} photons returned/atom/Joule transmitted, corresponding to no optical pumping (linearly polarized), or 8.9×10^{-8} with optical pumping (circularly polarized).

N_c = sodium column density (4.3×10^9 atoms/cm^2)

T_A = atmospheric transmittance at 589 nm at zenith (0.67 from MODTRAN, 0.59 estimated from measurements)

T_u = uplink transmittance of sodium guidestar telescope (0.80)

T_d = downlink transmittance at 589 nm through AEOS (0.23 for the results below)

QE = WFS quantum efficiency (0.74 for the results below)

P_L = laser power at 589 nm (40 W for the results below)

D_{subap} = subaperture width (30 cm referred to output space for the results below)

τ_{int} = integration time of WFS (1 to 2 msec for the results below)

Because circularly-polarized light is used, optical pumping is expected to occur, so the leading factor C_{Na} is equal to 8.9×10^{-8} photons returned/atom/(Joule transmitted). It should also be noted that the downlink optics transmittance seems low, only 0.23. This accounts for the 56% transmission from the primary mirror through 6 other mirrors and an uncoated fused silica (Infrasil) window to the optics room, plus 8 optics with a 95% transmittance at 589 nm each in the high-power path, plus another 15 optics with ~ 98 % transmittance each in the low-power path, plus a lenslet array with 90% transmission and a 10-nm bandpass filter with 90% transmission. These numbers include degradation due to contamination. The resulting optical-path transmission is about 23%. The other input to Eq. (1) that may be varied is the integration time, which experimentally is varied from 1 msec for 1000 Hz frame rate to 2 msec for 500 Hz on the AWFS. There are times when 250 Hz is used also.

(1) assumes operation at zenith, with the mean beacon backscatter altitude of 90 km above mean seal level. This basic equation should be modified when operation is off zenith. The modified formula (which does not yet include all degraders) is

$$S_{Na0}(\theta_{zen}) = C_{Na}\, [N_c/\cos(\theta_{zen})]\, T_A^{2/\cos(\theta zen)}\, T_u\, T_d\, QE\, P_L\, D_{subap}^2\, \tau_{int}\, \cos^2(\theta_{zen}). \quad (2)$$

The factor $N_c/\cos(\theta_{zen})$ comes from the greater depth of the sodium layer when the laser traverses it an angle θ_{zen}. The factor $T_A^{2/\cos(\theta zen)}$ arises because of the increased path through the atmosphere when propagating round-trip at angle θ_{zen}, with a flat-earth approximation. The factor $\cos^2(\theta_{zen})$ is needed because there is an implicit 1/range^2 in Eq. (1), and the range increases as $1/\cos(\theta_{zen})$ for off-zenith operation. Note that Eq. (2) is intended to be valid for zenith angles less than 45°. For larger zenith angles the effect of a round earth are important and affect the zenith-angle dependence. There is also the possibility of variable range to the sodium later, for which the mean range has been observed to range from 85 to 110 km [17].

Next, the degraders are discussed. First the sodium layer column content can vary to lower values. Values as low as ½ the nominal value given above (4.3×10^9 atoms/cm^2) are observed frequently [17]. This will be accounted for below. The atmospheric transmission is also observed to vary. As will be seen below, observations of reference stars in the I band (700-900 nm) over time, the atmospheric transmission scaled to 589 nm at can vary down to about 0.50 scaled to zenith during data collects, as will be seen in the next section. This corresponds to a 75% reduction from a nominal atmospheric transmission of 0.67 at 589 nm. The round-trip impact is therefore 0.56 which is almost a factor of 2 at zenith.

The impact of geomagnetic fields is to reduce optical pumping, and thus signal return. This is studied in detail in [14]. Fig. 12 of that document pertains to Maui conditions. From that figure, the approximate reduction in signal due to geomagnetic fields is about $F_{Geo} = 0.6$ when averaged over azimuth and zenith angles from 0 to 45 degrees.

The accuracy in this estimate is about 15%. Given the large variability due to other degraders, such as sodium layer density and atmospheric transmission, a 15% accuracy in the geomagnetic effect is not critical.

Population saturation can have a significant impact. The degradation due to population saturation is given by [8]

$$F_{sat} = 1/(1 + I_0/I_{sat}), \quad (3)$$

where

$I_0 = P_L / A_{laser}$,

P_L = laser power at 589 nm (40 W), as given above,

A_{laser} = the laser FWHM area at altitude = $(\pi/4)[D_{spt,\,0}/\cos(\theta_{zen})]^2$,

Dspt, 0 = spot diameter at 0° zenith, = 68 cm based on measured spot width of 7.5 μrad on AWFS,

$I_{sat} = h\nu/(2\sigma\tau_{Na})$,

$h\nu$ = the photon energy at a wavelength of 589 nm (3.36×10^{-19} J),

σ = the sodium atom cross section (1.1×10^{-13} m^2 from Eq. (5.8) of [13]), and

τ_{Na} = the sodium atom relaxation time at altitude (16 nsec [2, 13]).

It should be noted that there are a few different numbers for the sodium atom cross section for the D_2 line, varying up or down 50% from the above number [1, 2, 13]. Putting in the numbers for I_0 and I_{sat} one obtains 109 and 93 W, respectively, at zenith. The loss factor due to saturation of the sodium layer therefore is about 0.46 at zenith and improves to 0.63 at 45° zenith, because the spot size grows larger for larger zenith angles, reducing the laser intensity.

In addition to the above, there is also the effect of imperfect polarization of the laser, off-resonance operation, atomic recoil, and collisions [2]. Each of these effects may cause a degradation in the range of 0 to 10%. Choosing a nominal degradation of 5% due to each of these effects results in a degradation factor of $F_d = (1 - 0.05)^4 = 0.81$. This factor could easily be 0.6, given the various uncertainties in the spot profile at altitude and laser properties. The resulting more complete formula for the estimate of signal is then

$$S_{Na}(\theta_{zen}) = S_{Na0}(\theta_{zen})\, F_d\, F_{sat}\, F_{Geo}. \quad (4)$$

The above calculations are summarized in Fig. 3. The upper left plot shows the basic result with the nominal sodium layer density and also with the density divided by 2. A 1 msec AWFS integration time (~1 KHz frame rate) is assumed. The upper right plot shows the same result with a 2 msec integration time (~500 Hz frame rate). The lower plots show the corresponding results with all the aforementioned degraders included (geomagnetic factor, saturation factor, lower atmospheric transmission, laser detuning, laser polarization, atomic recoil, and atomic collisions).

One may convert the above numbers to photons/sec/cm^2/W at zenith at the pupil with unity atmospheric transmissivity and circularly polarized light. In the nominal case, this is just $C_{Na}\, N_c$. One obtains 382 photons/sec/cm^2/W for the nominal sodium column density, and 191 photons/sec/cm^2/W for ½ the nominal column density. For the computations that include degradations, the corresponding numbers are 86 and 43 photons/sec/cm^2/W, respectively. The low signal result is 22.6 % of the nominal signal result due to a factor of 0.46 due to saturation, a factor of 0.6 due to geomagnetic effects, and a factor of 0.8 due to the four effects discussed in the previous paragraph.

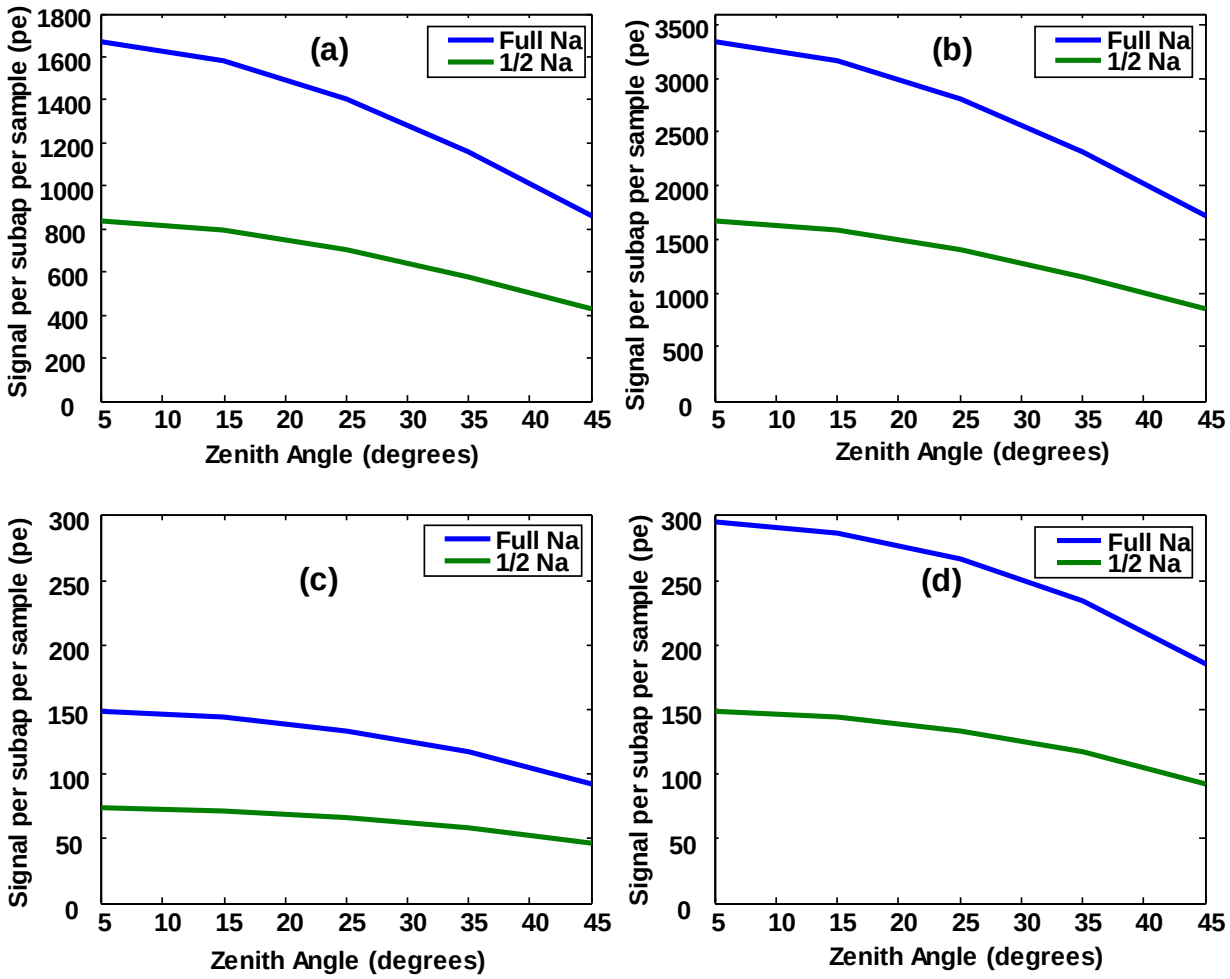

Fig. 3. Signal per subaperture per time sample versus zenith angle. (a): AWFS integration time = 1 msec, nominal and ½ the nominal sodium density. (b): AWFS integration time = 2 msec, nominal and ½ the nominal sodium density. (c): same as (a) but with all degraders. (d): same as (b) but with all degraders. Note the different scales for the y-axis for the different figures.

3. MEASURED SIGNAL RETURNS

The measured returns are a significant function of atmospheric transmission. Atmospheric transmissions are computed based on observed signal levels from calibration stars. A month-by-month summary of atmospheric transmissions are given in Table 1. The transmissions are converted to zenith by using $T_{zen} = T(\theta)^{\cos(\theta zen)}$, where θ_{zen} is the zenith angle of the measurement. The expected value at zenith is 73% based on MODTRAN calculations in the 700-900 nm band, and 67% at 589 nm. Hence, one should scale the numbers in Table 1 by a factor of 67/73 = 92% to estimate transmittance at 589 nm at zenith. Using the mean value of Table 1 of 64.8 % in the I band and scaling to 589 nm gives a mean value of 59.5% at zenith at 589 nm, on average. This atmospheric transmittance is used in the calculations for the final comparison. The measured result may be somewhat lower than the MODTRAN result because of the consistently wetter weather than normal experienced in 2018.

Table 1. Atmospheric transmission by month, March 2018 to March 2019 (normalized to zenith), measured in the 700-900 nm band.

Month/Year	Average Atmospheric Transmission (T_{atm})	Standard Deviation of T_{atm}
3/18	0.63	0.05
4/18	0.68	0.06
5/18	0.62	0.04
6/18	0.71	0.05
7/18	0.73	0.05
8/18	0.70	0.07
9/18	0.65	0.05
10/18	0.64	0.04
11/18	0.64	0.04
12/18	0.67	0.06
1/19	0.58	0.08
2/19	0.53	0.06
3/19	0.64	0.08

The measured results involved a judicious thresholding of signal versus noise in each subaperture, and a well-calibrated estimate of the relationship between digital counts and detected photoelectrons (0.24 electrons/count) as well as non-uniformity corrections. The signal levels are averaged over all active subapertures and also averaged over all frames in a data set (usually of the order of 1000 frames per data set). The standard deviation is computed in a similar manner based on this long vector of subaperture measurements. Next, the measured radiometry per subaperture is compared against the computations above. A summary is shown in tabular form by month in Table 2 and in graphic form in Fig. 4. There are 4 sub-figures in Fig. 4. Each shows a plot for each of 2 or 3 consecutive months. The data is normalized to 500 Hz frame rate.

Table 2. Measured signal returns (pe/subaperture/sample) by month, March 2018 to March 2019.

Month/Year	Mean (pe/subaperture/sample)	Standard Deviation (pe/subaperture/sample)
3/18	51.57	35.9
4/18	82.52	68.0
5/18	54.18	25.9
7/18	48.12	22.9
9/18	57.46	28.9
11/18	84.13	23.2
12/18	175.10	36.7
1/19	95.60	73.0
3/19	96.13	36.1

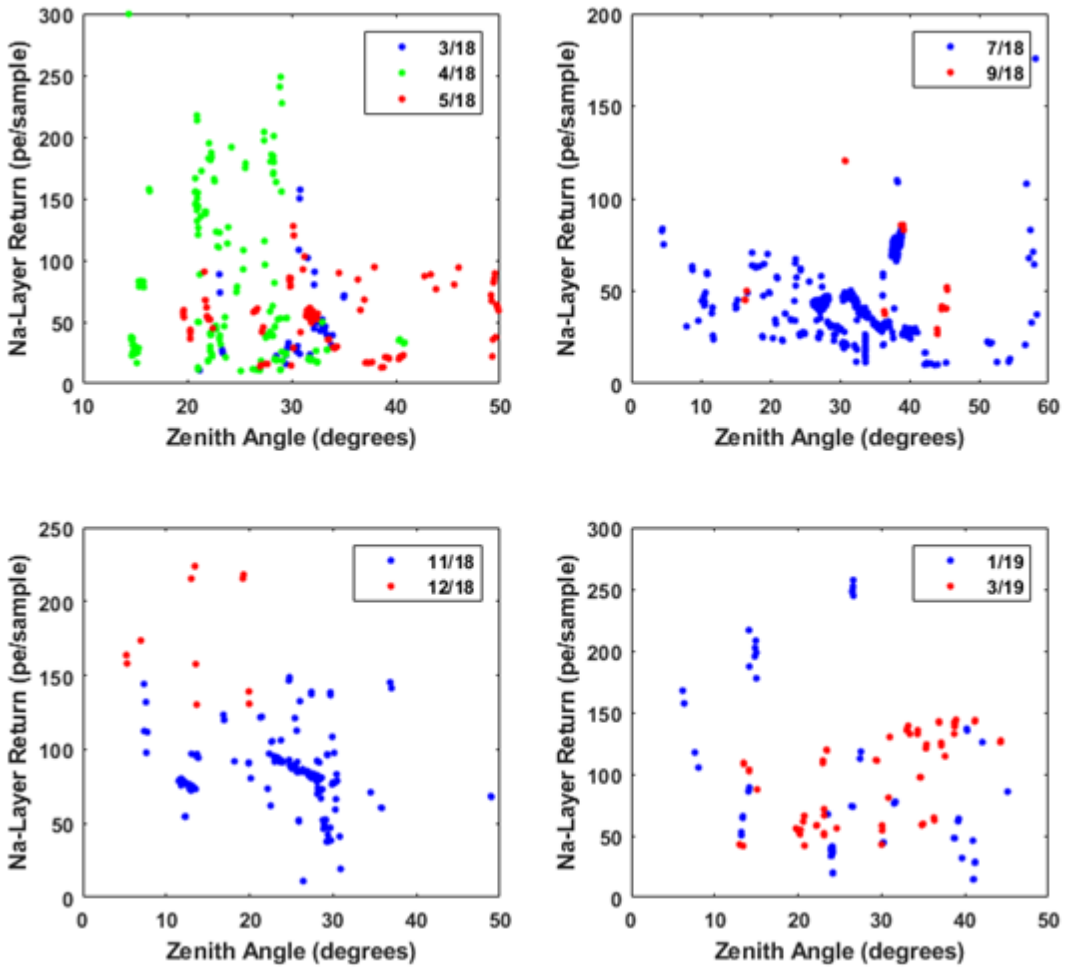

Fig 4. Measurements of LGS signal return per subaperture at 40 Watts laser power, normalized to 500 Hz frame rate. (a): March-May 2018. (b): July-September 2018. (c): November-December 2018. (b) January-March 2019. Each point represents the average of a single data set.

The results of Table 1 and Figure 4 show a monthly variation that is similar to those reported by others, with a mean return in the winter months that is a factor of two to three times higher than in the summer months. The severe impact of all the losses, including saturation, geomagnetic fields, two-way atmospheric transmission and optical path transmission, are evident. The mean signal can be computed from the mean of the monthly averages in Table 2, resulting in 82.8 pe per subaperture per 2 msec sample. The median value of these numbers is 82.5. The standard deviation is 39. This should be compared with the zenith-averaged values of the lower curve of Figure 3d, which yields 126 pe per subaperture per 2 msec sample. The comparison of 83±39 per versus 126 from theory indicates that the theory is at 1.10 standard deviations from the measured values. The measured mean is about 83/126 = 65.9 % of the theory with degradations included, and similarly for the measured median.

4. DISCUSSION

The above measurements show that the signal levels are at the low end of that expected from a narrow-line laser. The measured results are typically about 66% of theory with degradations (see plot (d) of Fig. 3 and compare to Fig. 4). There are many contributors which could result is this difference from the computed value. For example, if each optic in AEOS had a 1% lower transmission than quoted above, the computed value would be 30% lower. If the laser was detuned from resonance, one could easily reduce the measured value by a factor of 2. The potential

detuning of the laser was rarely checked, and this is a potential suspect for the discrepancy. Since the mean measured atmospheric transmission was used in the theory calculation with degradations, the atmospheric transmission is likely not a part of the explanation, at least to lowest order. There is also the issue of D_{2a} and D_{2b} population transfer with very narrow laser lines. This could be part of the explanation, but is not addressed further here.

The above measured median signal level, about 57 pe, is satisfactory for AO operation with the low-noise cameras that are used. A signal level of 83 pe results in a shot-noise-limited signal-to-noise ratio of about 9.1, which is sufficient with margin for the assumed 30 cm subapertures and 500 Hz frame rate. This subaperture size and frame rate is sufficient for good correction in the K band. However, a desirable signal level for high-quality wavefront correction in the visible or near IR is about 2 to 8x the level measured in the previous section. A factor of two improvement would support sampling at 1 KHz rather than 500 Hz, and another factor of 4 would support 15 cm subapertures rather than 30 cm subapertures for the better correction that is needed in the visible or near IR.

To obtain such improvements, the laser line may be broadened or chirped in frequency. With this approach, additional atoms in the inhomogeneously-broadened line will become accessible [18], and the resulting signal improvement ratio over Eq. (3) is estimated by

$$R_s \sim [\Delta\nu_{Na} + \min(\Delta\nu_L, \Delta\nu_D)]/ \Delta\nu_{Na,} \quad (5)$$

where

$\Delta\nu_{Na}$ = sodium natural linewidth (62 MHz FWHM),

$\Delta\nu_L$ = laser linewidth (0.1 MHz or less),

$\Delta\nu_D$ = Doppler linewidth (1100 MHz FWHM).

The formula (5) is valid when $\Delta\nu_L < \Delta\nu_D$. Hence if the laser linewidth were broadened or chirped over about 1.0 GHz FWHM, one should expect a factor of roughly (1100 MHz)/(62 MHz) = 17.7 improvement in signal. Furthermore, this chirped line should be imposed roughly every 16 nsec to ensure that each atom can be fully utilized, i.e., so that each atom can be pumped to the excited state not long after it decays. The implied chirp rate is 1GHz/16 nsec, which requires a total phase modulation of (1GHz)(16 nsec)/2 = 8 waves. This approach would also reduce saturation of the Sodium D_2 line as well. Thus, there are means for obtaining the desired factor of 8 or more higher signal levels for a more robust AO system based on a sodium laser guidestar.

5. SUMMARY AND RECOMMENDATIONS

The measured radiometry for returns from the sodium layer are typically about 66% of the degraded nominal expectation of Fig. (3d). These signal levels are approximately what are needed for good wavefront correction in the K band but are lower than desired for good wavefront correction in the I-band. Based on the above analysis, atmospheric transmission, saturation of the sodium population, and geomagnetic effects are significant causes of signal loss for the sodium beacon. Operation of the laser on the peak of the sodium line should be checked more regularly. Not much can be done about atmospheric transmission, except possibly a larger laser. A larger spot size could also improve signal by reducing saturation but will also increase anisoplanatism. Not much can be done about the geomagnetic effect. One further means for increasing the sodium return is to broaden the laser linewidth to about 1.0 GHz. This approach could increase signal by a factor of up to 17.

6. REFERENCES

[1] W. Happer, G. J. MacDonald, C. E. Max, and F. J. Dyson. Atmospheric-turbulence compensation by resonant optical backscattering from the sodium layer in the upper atmosphere, *J. Opt. Soc. Am. A*, 11(1):263-276, 1994.
[2] P. W. Milonni, H. Fearn, J. M. Telle, and R. Q. Fugate. Theory of continuous-wave excitation of the sodium beacon, *J. Opt. Soc. Am. A*, 16,(12):2555-2566, 1999.
[3] A. Flusberg, AVCO Research Labs Tech Memo, 1985.
[4] M. C. Roggemann, B. M. Welsh, and R. Q. Fugate. Improving the resolution of ground-based telescopes, *Rev. Mod. Phys.*, 69(2):437–505, 1997.

[5] J. M. Beckers. Adaptive optics for astronomy: principles, performance, and applications, *Ann. Rev. Astron. Astrophys.*, 31(1):13–62, 1993.
[6] N. Hubin and L. Noethe. Active optics, adaptive optics, and laser guide stars, *Science*, Vol. 262, pp. 1390–1394, 1993.
[7] M. Lloyd-Hart, J. R. P. Angel, B. Jacobsen, D. Wittman, R. Dekany, D. McCarthy, E. Kibblewhite, W. Wild, B. Carter, and J. Beletic. Adaptive optics experiments using sodium laser guide stars, *Astrophys. J.*, 439(2):455–473, 1995.
[8] C. E. Max, S. S. Olivier, H. W. Friedman, J. An, K. Avicola, B. V. Beeman, H. D. Bissinger, J. M. Brase, G. V. Erbert, D. T. Gavel, K. Kanz, M. C. Liu, B. Macintosh, K. P. Neeb, J. Patience, and K. E. Waltjen. Image improvement from a sodium-layer guide star adaptive optics system, *Science*, 277(7):1649–1652, 1997.
[9] M. Lloyd-Hart, J. R. P. Angel, T. D. Groesbeck, T. Martinez, B. P. Jacobsen, B. A. McLeod, D. W. McCarthy, E. J. Hooper, E. K. Hege, and D. G. Sandler. First astronomical images sharpened with adaptive optics using a sodium laser guide star, *Astrophys. J.*, 493(3):950–954, 1998.
[10] P. Wizinowich. Astronomical Science with Adaptive Optics at the W. M. Keck Observatory, *Pub. Astro. Soc. Pac.*, 125(3):798–808, 2013.
[11] Subaru Telescope, https://www.naoj.org/Pressrelease/2006/11/20/index.html, 2006.
[12] M. Enderlein, W. G. Kaenders, and D. Bonaccini-Calia. Adaptive Optics: ESO's Very Large Telescope sees four times first (laser) light, *Laser Focus World*, July 2016.
[13] D. A. Steck. Sodium D Line Data, Los Alamos Tech Note (Rev 14 October 2003).
[14] J. Drummond. 2006 Summary of 50 W Fasor Sky Tests and Model Summary, Technical Memo, Fig. 12, February 2007.
[15] M. D. Abercrombie. Initial Results from Sodium Guide Star Testing at AMOS, Amos Tech Memo, July 6, 2017.
[16] E. Walker, J. Mathis, and G. Balinbin. Optical Characterization Work Summary of Launch Telescope, AMOS Tech Memo, January 2018.
[17] L. C. Roberts, Jr., W. L. Bradford, C. R. Neyman, and A. Z. Liu. Measurements of Mesospheric Sodium Abundance above the Hawaiian Islands, *Pub. Astron. Soc. Pac.*, 119(2):787–792, 2007.
[18] O. Svelto. *Principles of Lasers*, (1st Edition), D. C. Hanna, ed., pp. 58-78, Plenum Press, 1982.
[19] D. L. Fried. Optical Resolution through a Randomly Inhomogeneous Medium for Very Long and Very Short Exposures, *J. Opt. Soc. Am.*, 56(10):1372-1379, 1966.

APPENDIX A: ANALYSIS OF SUBAPERTURE SPOT SIZE ON WFS

The spot size on the AWFS is the convolution of the beacon spot at altitude and the downlink divergence. It is well known that the beacon spot is approximately Gaussian for a focused and mildly aberrated uplink beam. It is also well-known that the downlink atmospheric aberrations cause a spot that is approximately Gaussian on average. Using the property that the convolutions of a Gaussians are also a Gaussian with a width that is the root-sum-square of the individual Gaussians, one obtains

$$\Delta\theta_{spt} = [\Delta\theta_{bcn}^2 + \Delta\theta_{atm}^2]^{1/2}, \quad \text{(A1)}$$

where $\Delta\theta_{spt}$ is the full-width at half max (FWHM) of the spot size in a subaperture of the AWFS, $\Delta\theta_{bcn}$ is the FWHM angular width of the beacon at altitude as seen from the telescope, and $\Delta\theta_{atm}$ is the FWHM of the short-exposure point spread function (PSF) due to the atmosphere. The latter is given by [19]

$$\Delta\theta_{atm} = \lambda/(3.4r_0) \sim (0.589\text{x}10^{-6}\text{ m})/(3.4*0.12\text{ m}) = 1.44\ \mu\text{rad}. \quad \text{(A2)}$$

This result is for nominal conditions. The angular width could be much larger. The angular spot size of the beacon as seen from the telescope is given by divergence of the uplink beam. This uplink divergence consists of the LGS optics, the atmosphere, and diffraction due to the exit aperture. The uplink diameter of the beam as it leaves the optical system is 23 cm, at exp(-2) intensity at full width. It is known that the uplink aberration on the LGS optics after adjustment is about 0.16 waves root-mean square (RMS) at 633 nm [16], primarily comprising the principal aberrations. Next, use the approximation that the FWHM beam spread relative to diffraction-limited is given by

Strehl$^{-1/2}$ = exp($<\Delta\phi^2>/2$), where $<\Delta\phi^2>$ is the spatial RMS phase error in radians at the sodium laser wavelength. The angular beam spread due to LGS optics is then

$$\Delta\theta_{LGS\ opt} = \lambda/(DS^{1/2}) = (\lambda/D)\ \exp(\Delta\phi^2/2) = (2.56\ \mu rad)(1.65) = 4.22\ \mu rad. \quad (A3)$$

This angular spread should be combined with the uplink short-exposure beam spread due to atmospheric aberrations, $\Delta\theta_{atm}$, which is just as computed above. The optical and atmospheric aberrations are typically combined in root-sum-square as above, so the LGS angular spread at altitude, as seen by the telescope, is

$$\Delta\theta_{bcn} = [\Delta\theta_{LGS\ opt}{}^2 + \Delta\theta_{atm}{}^2]^{1/2} = [4.22^2 + 1.44^2]^{1/2} = 4.45\ \mu rad. \quad (A4)$$

Hence, referring back to Eq. (A1) gives the total spot angular diameter as seen at the AWFS:

$$\Delta\theta_{spt} = [\Delta\theta_{bcn}{}^2 + \Delta\theta_{atm}{}^2]^{1/2} = \quad [4.45^2 + 1.44^2]^{1/2} = 4.7\ \mu rad. \quad (A5)$$

Given the result of Eq. (A5) and that the pixel angular width of the AWFS is 3.0 μrad in output space, the expected width of the LGS spot at FWHM is about 1.5 pixels in output space. What is actually observed is somewhat worse than this, typically the observed spot is about 2.5 pixels in width, as shown on the right of Fig. 2. The observed spot width on the AWFS of 7.5 μrad spot width referred to output space, and this equates to a 68 cm beacon spot width at a range of 90 km (0 degrees zenith). It should be noted that the beacon spot width automatically scales for off-zenith cases to larger physical widths, in proportion to range, and this will keep the apparent angular extent the same at the AWFS. That is, if the divergence θ_L on the exiting laser beam is kept constant versus zenith, then the beam diameter at altitude will be $D_{spot} = \theta_L R/\cos(\phi)$ as a function of zenith angle ϕ, and the resulting apparent spot size at the AWFS will be $D_{spot}/[R/\cos(\phi)] = \theta_L$, so that the apparent angular extent is approximately constant versus zenith angle (neglecting the zenith effect on intervening atmospheric turbulence).